

## Digital twin of USV thruster based on CFD simulations and towing tank experiments



Krisztián Kiss-Nagy\*, Győző Simongáti

Department of Aeronautics and Naval Architecture, Faculty of Transportation Engineering and Vehicle Engineering, Budapest University of Technology and Economics, Műegyetem rkp. 3., H-1111 Budapest, Hungary

### ARTICLE INFO

#### Keywords:

Underwater thruster  
3D printed thruster  
Digital twin  
CFD  
Unmanned Surface Vehicle (USV)

### ABSTRACT

Unmanned or Autonomous Surface Vehicles (USV/ASV), Remotely Operated and Autonomous Underwater Vehicles (ROV/AUV) are becoming widely used in industry, environmental monitoring and scientific research. In practice, it is often not feasible, or it is too dangerous to test and tune USVs equipped with expensive instruments and sensors particularly in high current environments. Realistic simulations are increasingly important, especially in hazardous operating conditions such as flooding river, catastrophe, bad weather conditions, heavy traffic, etc. The aim of this work was to create the digital twin of a 3D printed underwater thruster that is easily available and simple to manufacture. Transient Computational Fluid Dynamics (CFD) simulations were used to model the hydrodynamic forces acting on the thruster. This aims to enable the modelling of similar but different thruster geometries in the future, without the need for real experiments. In order to validate the CFD simulations and the final digital twin, open water propeller tests of the thruster were performed in a small towing tank. Underwater brake test bench measurements of the permanent magnet synchronous motor (PMSM) driving the thruster was also required to properly model the propeller-motor interaction. The validated thruster digital twin created in this paper can be used for realistic and safe simulations of USVs or can be run on an on-board computer for diagnostic and prediction tasks.

### 1. Introduction

Unmanned surface or underwater vehicles (USV/AUV) are getting more and more widely used in industry, scientific research and environmental monitoring. There are several examples of the application of these vehicles in seabed and riverbed mapping [1-3], water velocity measurement [4, 5] and water quality measurement [6, 7] both in sea and inland water environments. The main advantage of these applications is that it is not necessary to operate a complete vessel or boat with the appropriate crew, but only a small USV or AUV is needed to autonomously perform the monotonous, time-consuming and sometimes dangerous task, even without supervision. Such small vehicles are almost always electrically powered, and propulsion is often achieved with ducted, podded plastic thrusters as in [8, 9]. In several cases, rapid prototyping has been implemented, for example using 3D printed propellers [10] or fully 3D printed AUVs [11]. A unique

\* Corresponding author.

E-mail address: [kiss-nagy.krisztian@edu.bme.hu](mailto:kiss-nagy.krisztian@edu.bme.hu)

development was made in [12] by developing a small diameter plastic contra-rotating thruster for marine robots.

The objective of this study is to create the digital twin of a simple and inexpensive to manufacture Fused Filament Fabrication (FFF) 3D printed underwater thruster with easily variable Computational Fluid Dynamics (CFD) simulations validated by towing tank experiments. The digital twin, implemented in a realistic simulation environment, will allow to tune and improve the control system of USVs or AUVs and to estimate the required battery capacity to perform specific tasks. Diagnostic and predictive functions can also be implemented by using the digital twin on the on-board computer of the vehicle. Similar task has been implemented in [13] where high-precision digital twin of a ship cooling pump has been created for monitoring and fault diagnosis tasks. In USV applications multihull configurations are very popular, where the use of differential thrust steering is obvious due to simplicity. This has been investigated in several studies, for example [14] studied the effect of thruster arrangement on the manoeuvrability of USVs, or [15] performed dynamic modelling of a USV equipped with rudderless twin thrusters. In order to ensure reliable and robust operation of differential steering (and other under-actuated) USVs, simulation in a safe environment is essential. The hydrodynamic and energetic models describing the thruster are crucial components of realistic simulations in terms of manoeuvrability, energy consumption and range estimation.

For the hydrodynamic modelling of the thruster, CFD simulations have been performed. Several examples on this topic can be found in the literature. In [16], CFD study of an azimuth, ducted thruster was performed, where the aim was to create a new virtual disk model that considers the lateral forces and the effect of the nozzle. Unsteady Reynolds-Averaged Navier Stokes (URANS) solver with  $k-\omega$  SST turbulence model was applied and the propeller rotation was modelled using the Sliding Mesh (SM) method. Similar methods (RANS, SST, SM) were used in [17] to study Podded propulsors in manoeuvring conditions. Steady Moving Reference Frame (MRF) and unsteady SM methods were compared in [18] for the investigation of ducted propellers. The study showed that the static MRF method gives reasonable accuracy in the trawling, medium advance ratio and free sailing conditions ( $j=0.2-0.6$ ), but in bollard condition ( $j = 0$ ) it may be necessary to use the SM method. A Rim-driven Thruster (RDT), which is quite similar to the thruster studied in this paper, was investigated in [19], where CFD was used to optimize the geometry of the duct. Static RANS equations and MRF method were used for the CFD simulations, and the optimization resulted in an efficiency increase of 3-10 % depending on the advance coefficient. Open water CFD simulations of a conventional ducted propeller were carried out and the self-propulsion characteristics of an underwater vehicle with RDT were determined in [20] using static MRF and non-static SM methods. Hub-type and hubless RDTs were compared in [21] using MRF method and the results indicate clearly that hubless thrusters have higher efficiency. In this study, the reason for using CFD in addition to towing tank measurements is to allow the hydrodynamic modelling of thrusters with other geometries in the future without experiments.

Extensive energetic modelling of USVs has been carried out in [22] and the resulting energy consumption model has been integrated into the Gazebo simulation environment. For underwater robots minimal energy consumption is particularly important, thus [23] investigated the hydrodynamic shape optimization of a small Remotely Operated Vehicles (ROV), while [24] worked on the optimal control of a positive buoyancy diving autonomous vehicle to achieve a longer range. To improve ship motion prediction, a four-quadrant hydrodynamic propeller model of a submarine was created in [25] using CFD studies. Using also four-quadrant propeller curves [26] created a propeller torque observer and validated it with towing tank tests. In the present study to describe the operation of the brushless Permanent Magnet Synchronous Motor (PMSM) and its interaction with the propeller, underwater brake test bench measurements were performed, since water can enter between the stator and the rotor as in [27]. A similar design of submersible pump has been extensively studied in [28] highlighting that corrosion protection and adequate insulation are key issues for similar applications.

The main purpose of the newly developed digital twin is to enable safe and efficient simulation and tuning of small differential thrust steered catamaran USVs designed for hydrographic measurements and tasks (river current speed measurement, towing underwater sensors and pumps, sediment collecting etc.). Realistic simulation of marine vehicles is covered by several research projects, but there are a growing number of

examples where the open-source Gazebo simulation environment was used. Gazebo has been used to simulate the downstream mooring manoeuvres of river passenger vessels in [29]. A Gazebo based simulation environment has been developed in [30] for testing different types of USVs mainly in coastal and inland environments. Extensive simulation of catamaran USVs has been investigated in [31], while the performance of different control methods of USVs has been studied in [32], [33] and [34] in Gazebo environment. Based on these, the digital twin developed in this paper has been designed to be easily integrable into the Gazebo environment. To facilitate further utilisation of the digital twin, such as diagnostics, fault prediction, etc., the system is designed to be easily embeddable into the USV on-board computer.

## 2. Thruster geometry and components

The fundamental objective in designing the geometry of the thruster under study was to achieve a simple, reliable design with low maintenance requirements and which is easy to manufacture. FFF 3D printing was used for rapid prototyping. A low-cost, easily available brushless PMSM (D2836 750KV) was installed in the thruster, with stainless bearings and with waterproof coating on the windings. The concept is that the motor is completely submerged, allowing water to enter between the stator and the rotor. This circumstance increases the rotational resistance of the motor, but in this way the structure is extremely simple, no sealing or gearbox is required, and efficient cooling is ensured. The geometry of the propeller has been generated by an in-house fully parameterized MATLAB program, which is described in detail in a previous work [35]. The nozzle has a NACA6518 profile and can be mounted separately on the thruster to ensure easy modification. The specifications of the thruster are shown in Table 1, the design is shown in Figure 1, while the thruster used during measurements is shown in Figure 2.

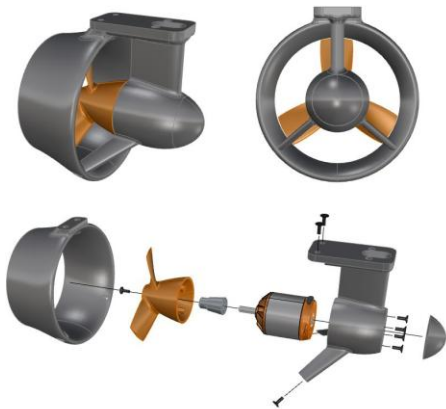


**Fig. 1** Concept of underwater thruster



**Fig. 2** FFF 3D printed thruster

**Table 1** Thruster specifications

Propeller diameter ( $D$ )	64 mm
Blade area ratio ( $A_D/A_o$ )	0.3
Design pitch ratio ( $P/D$ )	0.8
Rake	4°
Skew	0°
Number of blades ( $z$ )	3
Nozzle length	40 mm
Nozzle inner diameter	66 mm
Nozzle inner diameter	86 mm
Motor velocity constant ( $KV$ )	750 rpm/V
Motor max. amperage ( $I_{max}$ )	25 A

### 3. Towing Tank experiments

The Budapest University of Technology and Economics (BME), Department of Aeronautics and Naval Architecture (RHT) has a towing tank facility for small size measurements. The dimensions of the tank are limited (width: 1 m, water depth: 1 m, length: 16 m), but with sufficient care full scale measurements of the thruster can be carried out. The towing speed can be varied between 0.1 m/s and 3 m/s with an arbitrary speed profile. During the measurements, the water temperature was 15°C, the density ( $\rho$ ) was 997 kg/m<sup>3</sup>, no wave damping was applied, and there was a minimum 8-minute break between the towing tests.

#### 3.1 Experimental setup

During the measurements, the thruster was operated completely as it will be installed except for the presence of the hull. The PMSM was controlled by a 40 A bidirectional Electronic Speed Controller (ESC) which was powered by a 12 V LiPo battery. The thruster mounting was provided by an aluminium rod and a 3D printed mounting bracket. The angle of the thruster was adjusted with a servo but remained unchanged (0°) during the measurements. The measurement setup is shown in Figure 3. The propeller shaft of the thruster was 300 mm below the water surface. A custom designed ESP32 microprocessor based control, measurement and data acquisition system were used to perform the following tasks.

- Control of the ESC throttle [%] by generating a PWM signal (Pulse Width Modulation: 50 Hz square wave with a pulse width between 1000  $\mu$ s and 2000  $\mu$ s, which can be equivalent to -100 % to 100 % throttle).
- Control of the servo with PWM signal that adjusts the angle of the thruster ( $\alpha$  [°]: from -90° to 90°).
- Measurement of the towing carriage speed ( $u$  [m/s]) using a 600 pulse per revolution optical encoder mounted on a trailing wheel. Measurement resolution is 0.01 m/s after appropriate filtering.
- The longitudinal and transverse forces ( $X$  [N],  $Y$  [N]) were measured with strain gauges and two 24-bit Analog Digital Converter (ADC) and amplifier modules (HX711 IC). Measurement resolution is 0.01 N; sampling rate is 80 Hz.
- The measurement of the propeller rotational speed ( $n$  [Hz]) was carried out with an electronic rpm sensor which converted the voltage changes of the PMSM phase wires into pulses (18 pulses per revolution) and thus functioned as an encoder. The measurement resolution is 1.0 rpm after appropriate filtering.
- The current ( $I$  [A]) drawn by the ESC was measured using a HALL effect current sensor (ACS712 - max. 30 A) and a 16-bit ADC (ADS1115). The measurement resolution is 0.01 A; sampling rate is 80 Hz after appropriate filtering.
- To measure the power, the battery voltage ( $U$  [V]) was measured using a simple voltage divider circuit and a 16-bit ADC (ADS1115). The measurement resolution is 0.01 V, sampling rate 80 Hz after appropriate filtering.

The measuring system has been calibrated with certified measuring equipment. The resistance of the rod holding the thruster was measured individually without the thruster and the results were used to correct the open water propeller tests. In reality, our possibilities to study these interactions are rather limited. Due to the many different operating conditions tested, the only option to support the thruster is to fix it from above, axial support and measurement was not possible. Since the measuring load cells could not be placed in the immediate vicinity of the thruster, it was not possible to test it without the rod being present. Verification was carried out in the Bollard pull case with zero advance speed and the data showed good agreement with the CFD, so it was assumed that in this condition there is no noticeable effect of the rod on the thruster. Hence the rod effect was corrected by subtraction only, neglecting the non-linear effects, due to the lack of other options. The ratio between the measured resistance of the free-standing rod and the forces measured during open water experiments is not significant at low towing speeds, but at higher speeds ( $u > 1$  m/s) the results should be treated with caution. Further studies are needed to investigate this in more profound detail. This

procedure was considered appropriate for the purposes of this paper. It was not possible to measure the torque of the propeller shaft directly, but the torque can be estimated from the measured current using the motor torque characteristics. For this purpose, underwater brake test bench measurements were performed on the propellerless thruster using the same measuring and data acquisition system, but in this case the strain gauge was mounted on a Prony brake. The characteristics of the towing tank and the control and measurement system imposed certain limitations on the measurements. The ESC could only stably drive the thruster underwater at a minimum of 1000 rpm. This is further complicated by the fact that the ESC does not break the propeller rotation, so at higher speeds, when the throttle is low, the resulting reverse thrust can increase the propeller rotational speed. If the towing carriage is moving with a speed higher than 2 m/s there is not enough time to take a sufficient number of measurements due to the limited length of the tank and the maximum sampling rate of the HX711 ADC. Due to the width of the tank, oblique open water propeller tests are not recommended because the thruster pushes the water against the tank wall. The combined effect of these limitations is that the advance angle  $\beta$  (1), which combines the control parameters ( $u$ ,  $n$ ), can only be achieved within a limited range. The consequences of this are mainly noticeable during the CFD validation, but since there are similar  $\beta$  limitations on the real USV (max speed 3 m/s, same ESC and motor), it does not affect the quality of the modelling overall.

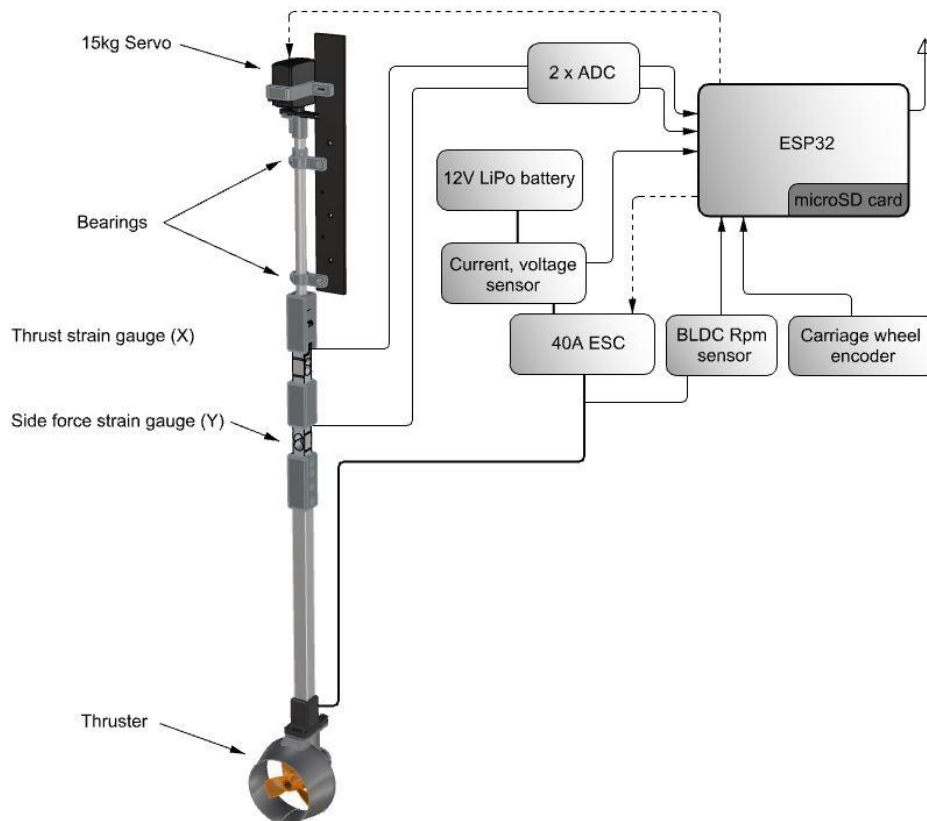


**Fig. 3** Podded thruster measurement setup

### 3.2 Open water propeller experiments

The evaluation of measurements and results has two basic objectives. Firstly, the experimental results will be used to validate the CFD simulations, and secondly, they will provide data for the creation of the digital twin. For the analysis of the measurements, the four-quadrant open water propeller characteristics variables and expressions (1) -(4) have been used. The thrust coefficient  $C_T$  and the torque coefficient  $C_Q$  could be expressed as a function of the advance angle  $\beta$  [°]. Note that for the post-processing calculations of  $\beta$ , the atan2 function was used as in [26].  $V_r$  [m/s] is the relative advance velocity,  $Q$  [Nm] is the propeller torque, which was calculated indirectly from the measured current.  $A_0$  is the area of the propeller disk, the other notations are given in the previous chapter.

$$\beta = \tan^{-1}\left(\frac{u}{0.7 \cdot D \cdot n \cdot \pi}\right) \quad (1)$$

$$V_r^2 = u^2 + (0.7 \cdot D \cdot n \cdot \pi)^2 \quad (2)$$

$$C_Q = \frac{Q}{0.5 \cdot \delta \cdot V_r^2 \cdot A_0 \cdot D} \quad (3)$$

$$C_T = \frac{X}{0.5 \cdot \delta \cdot V_r^2 \cdot A_0} \quad (4)$$

The open water ducted propeller tests were carried out at positive and negative towing speeds with the propeller rotating forwards and backwards, distinguishing four different operating conditions. The throttle was +/-50 % except for high-speed tows, where it was +/-20 % and 0 % to achieve higher  $\beta$ . The speed increased from -2 to 2 m/s with 0.2 m/s steps. For further use of the created digital twin (e.g. manoeuvre simulations, control system tests, on-board diagnostics) it is important to know the interaction characteristics between the ESC, motor and propeller, as this will determine the resulting working point (e.g. torque, rotational speed, thrust, current consumption). To describe the ESC and motor behaviour, the underwater brake measurements described earlier were performed. Note that the relationship derived from the measured data is only true for 12 V supply voltage (e.g. 3S LiPo battery) otherwise the speed-PWM correlation will change. In order to validate the motor-propeller interaction modelling extensively, dynamically varying towing experiments were also performed with linear variation of throttle and speed. Thus, with relatively few measurements, a comprehensive understanding of the characteristics of the thruster can be obtained. 12 measurements were carried out with the following parameters.

- At speed of 0 m/s varying throttle from 0 % to 100 % and from 0 % to -100 %
- Fixed speeds of 1 m/s and -1 m/s with varying throttle from 0 % to 70 % and from 0 % to -70 %
- At 50 % and -50 % throttle, varying speed from 0 m/s to 1.5 m/s and from 0 m/s to -1.5m/s
- At 0 % throttle, varying speed from 0 m/s to 1.5 m/s and from 0 m/s to -1.5 m/s.

For non-zero speed measurements, the boundary values were limited (max. throttle 70 %, max. speed 1.5 m/s) in order to avoid changing the input parameters too rapidly, which could potentially corrupt the measurements. Note that for more accurate results, static measurements are needed. The filtered and processed measurement results are compared with the output of the developed digital twin in section 6.3.

#### 4. CFD simulations

The main motivation for CFD based calculations is to provide a validated simulation method for accurate and relatively fast hydrodynamic modelling of pod thrusters. Since the main advantage of using CFD is that the geometrical variation is inexpensive, many different variants can be investigated and optimisation for a given task can be possible before production.

##### 4.1 Computational setup

For the CFD simulations, a URANS solver was used with the Ansys Fluent software. The flow around the propeller was modelled as a single-phase incompressible fluid with the material properties of water corresponding to the conditions of the towing tank ( $\rho$ , temperature, viscosity). The MRF method was used to model the propeller rotation. As recommended by [18], the SM method was also tested to increase the accuracy but was discarded due to the excessive computational demand (1° revolution per time step). For the purposes of this paper, shorter computation time is more important than accuracy. The SST  $k$ - $\omega$  model was used to model the turbulence around the thruster and for this  $y^+$  was kept to a maximum of 1 during the simulations.

There were two types of CFD simulation in this paper, one with fixed input ( $u$ ,  $n$ ) and the other with time-varying speed input ( $u(t)$ ,  $n(t)$ ). During the fixed input numerical open water propeller simulations, the rotational speed of the propeller was 2600 rpm or -2600 rpm, while the  $u$  speed was 0, +/-0.563, +/-1.126, +/-

1.690 and  $\pm 2.253$  m/s, resulting in a total of 18 measurement points. During the transient simulations, the time step was 0.005 s and, depending on the propeller operating mode, min. 5 s max. 12 s were simulated at one speed. Due to the extremely high computational time demand, it was not possible to use the  $1^\circ$  revolution/time step condition, so the chosen time step is a compromise between stability of the simulations and computational speed that is made for taking the aim of this paper into consideration.

In addition, to further increase the efficiency of the simulations in the future (measurement points per day), a slowly varying transient simulation was performed in each of the four possible operating modes ( $\pm u$ ,  $\pm n$ ). These time-varying speed input ('dynamic') simulations have been tuned based on the experimental data, resulting in the following input parameters:

- initial speed -1.5 m/s, rotational speed increases from 0 to 2600 rpm in 10 s, then speed increases to 0 m/s in 10 s ( $\beta = [-90^\circ, 0^\circ]$ )
- initial speed 1.5 m/s, rotational speed increases from 0 to 2600 rpm in 10 s, speed decreases to 0 m/s in 10 s ( $\beta = [0^\circ, 90^\circ]$ )
- initial speed -1.5 m/s, rotational speed decreases from 0 to -2600 rpm in 10 s, then speed increases to 0 m/s in 10 s ( $\beta = [-180^\circ, -90^\circ]$ )
- initial speed 1.5 m/s, rotational speed decreases from 0 to -2600 rpm in 10 s, then speed decreases to 0 m/s in 10 s ( $\beta = [90^\circ, 180^\circ]$ )

In all the dynamic cases, simulations start with a 5 s initialization with fixed input parameters to ensure a stable flow in the entire flow domain, giving a total of 25 s per simulation.

Cylindrical computational domain was used for the simulations with two separate regions. The outer flow region contains the fixed elements of the thruster, while the propeller is placed in a separate MRF region. The lateral surface of the outer flow region is a slip wall boundary, the front and back faces are velocity-inlet or pressure-outlet boundary conditions according to the direction of the velocity  $u$ . For the dynamically varying simulations, the Fluent frame motion method was used to vary the velocity, with the velocity defined as 0 m/s at the velocity-inlet boundary. The background domain and propeller region translational velocity, as well as the propeller rotational speed, were controlled by Fluent UDFs - User Defined Function (C code). The dimensions of the computational domain and the propeller surroundings are shown in Figure 4.

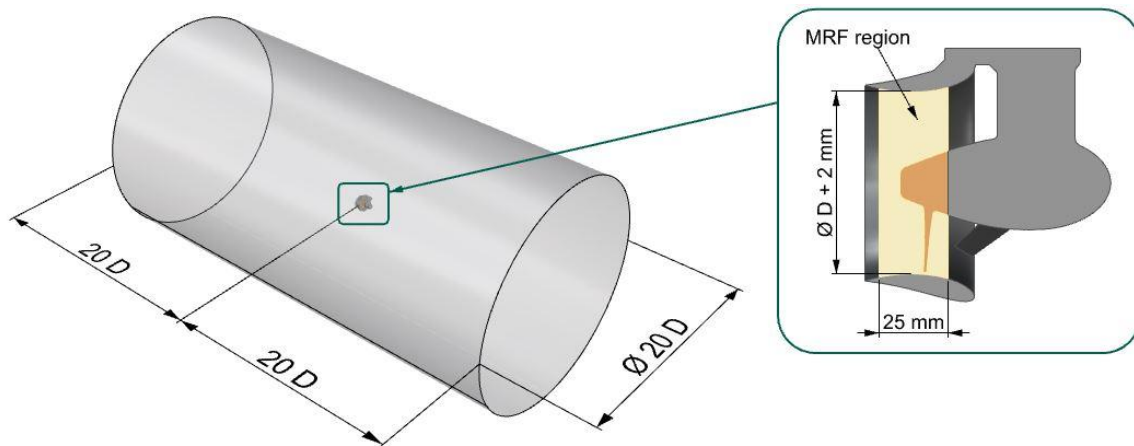


Fig. 4 Computational domain and MRF region

## 4.2 Mesh

Unstructured hexahedral mesh was generated using the OpenFoam open-source software, with the SnappyHexMesh utility. Several refinement zones have been applied around the thruster to capture the complex flow for all four propeller modes. Prismatic boundary layer cells have been applied to the entire surface of the thruster for accurate simulation of the boundary layer. Great care has been taken to create nearly equal cell sizes on the surface of the two flow regions (background, MRF region). To verify the mesh independence, 4 systematically refined meshes were investigated. The refinement ratio was  $\sqrt{2}$  in all directions. In these simulations, the speed was 0 m/s, and the rotation speed was  $\pm 2600$  rpm. The reason for

the negative speed is that in the case of an improper mesh, significant errors have occurred in this operating condition. The total thrust calculated for the 4 meshes is shown in Table 2 comparing the experimental and CFD results. To ensure accuracy, the fine mesh with 11-million cells was used for further simulations. Errors in the torque coefficient were not considered during the verification study because it was only possible to measure the torque indirectly. The final numerical mesh is illustrated in Figures 5 and 6.

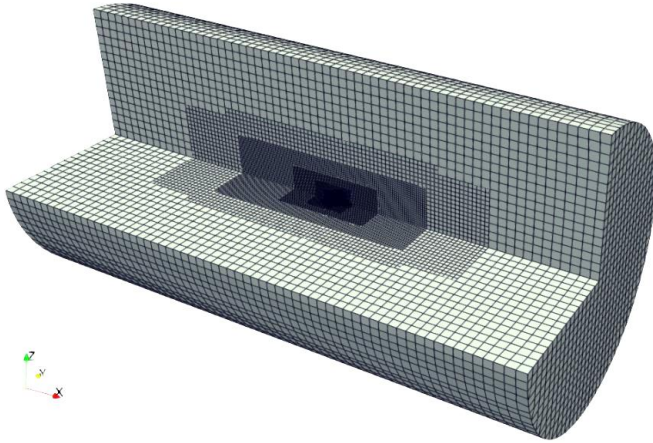


Fig. 5 Numerical grid used for the CFD calculations

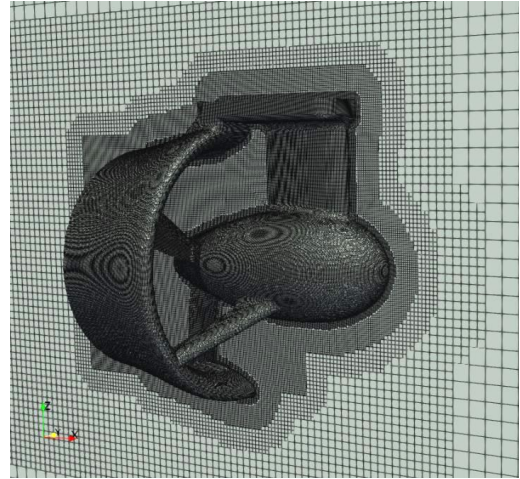


Fig. 6 Mesh around the propeller

Table 2 Mesh verification

Mesh	Cells [10 <sup>6</sup> ]	Experimental results $C_T$ [-]	CFD results $C_T$ [-]	Relative error
				$\frac{CFD - Exp.}{Exp.} \cdot 100 \%$
$\beta = 0^\circ$				
coarse	2.43	0.1487	0.1627	9.41
medium	5.13	0.1487	0.1589	6.86
fine	11.2	0.1487	0.1529	2.82
finest	22.7	0.1487	0.1527	2.67
$\beta = 180^\circ$				
coarse	2.43	-0.0729	-0.0648	-11.11
medium	5.13	-0.0729	-0.0686	-5.90
fine	11.2	-0.0729	-0.0704	-3.43
finest	22.7	-0.0729	-0.0718	-1.51

## 5. Experimental and numerical results

The results of the fixed input CFD simulations ('CFD') are presented and compared with the results of the towing tank experiments ('Exp.'), and the results of the time-varying speed input CFD simulations ('CFD dyn.'). In Figures 7 and 8, the  $C_T$  thrust coefficient and the  $C_Q$  moment coefficient are plotted as a function of the advance angle  $\beta$ .

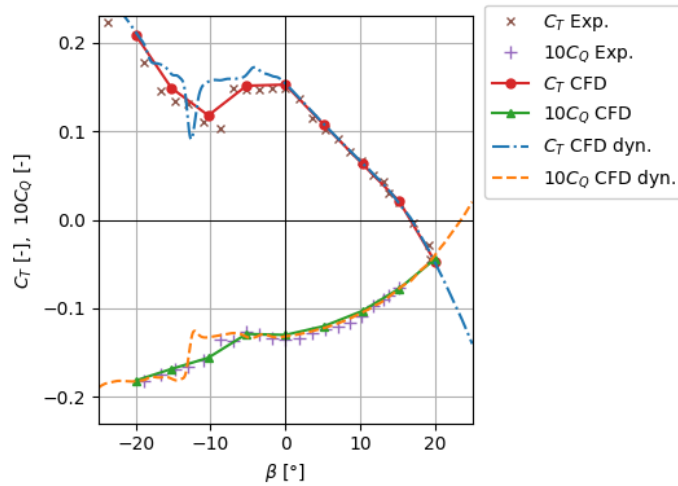


Fig. 7  $C_T$  and  $C_Q$  in range  $\beta = [-25, 25]$

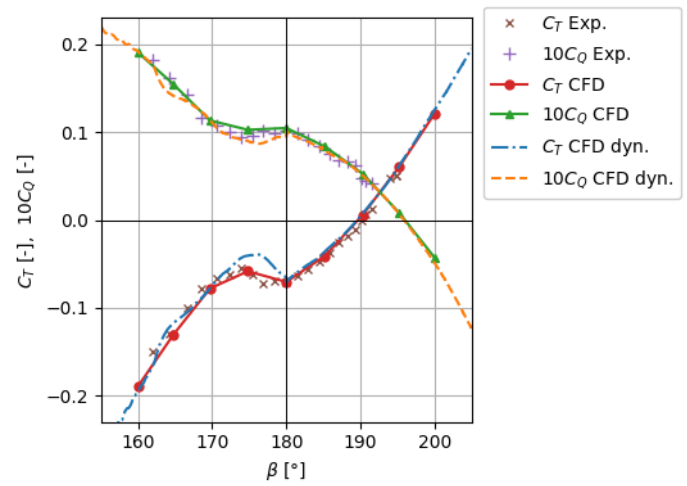
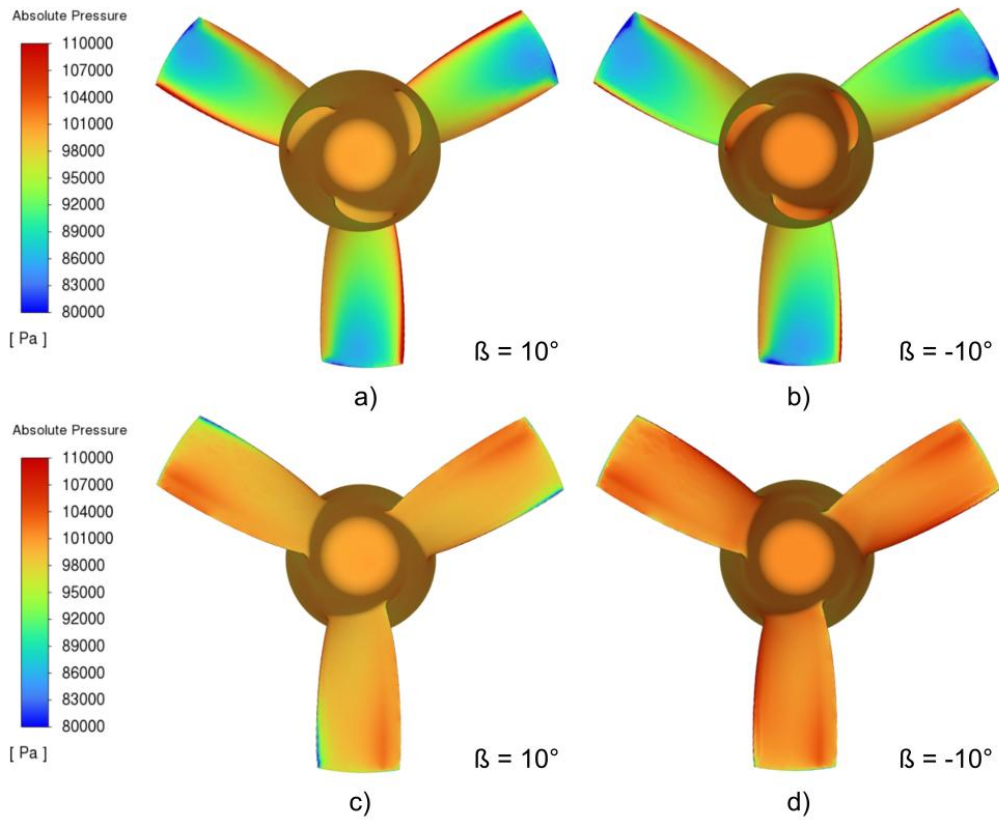


Fig. 8  $C_T$  and  $C_Q$  in range  $\beta = [155, 205]$

From the results, it can be concluded that when the sign of the advance speed and the propeller rotational speed are the same, the relative deviation of the  $C_T$  thrust coefficient from the experimental results is less than 5 % for both the systematic and dynamic CFD simulations. For different speed and rpm sign, this error is more significant, reaching up to 9 % for systematic CFD simulations. During the towing tank experiments, the range of  $\beta = [-20^\circ, 0^\circ]$  and  $[160^\circ, 180^\circ]$  showed the highest deviation in the measurement series, indicating that it is hard to reach a steady state flow in these operating conditions. Therefore, it is reasonable to conclude that CFD simulations require more time and a sufficiently fine mesh in this  $\beta$  range.

To enable a more profound analysis of the CFD results, the simulation at critical  $\beta = -10^\circ$  and the simulation at  $\beta = 10^\circ$  are compared below, where the latter shows an acceptable agreement with the measured data. Figure 9 compares the absolute pressure distribution on the pressure and suction sides of the propeller in these cases. Note that the propeller is rotating in the positive  $x$  direction with 2600 rpm in both cases. On the suction side of the propeller there is a difference in the pressure distribution at the leading edge of the propeller blades, especially at smaller radius, mainly due to the different velocity triangle and advance speed. Similarly, at the leading edge on the pressure side, it can be observed that the pressure variation at the blade tip is smaller in the case of  $\beta = -10^\circ$ , and the average pressure on the blade surface is clearly larger in this case. This is because the water accumulates on the pressure side of the propeller due to the negative advance speed of the thruster. Flow field in the XZ and XY planes for the two investigated cases is shown in Figure 10. The slight asymmetry of the resulting flow field is an indication of non-static flow conditions, which can be confirmed by the animation of the transient simulation results. The summed thrust, and within it the ratio of pressure and viscous forces generated on the duct and on the thruster bulb (motor casing, struts) are almost identical in both cases, due to the remarkable similarity of the velocity field ahead of the thruster. The only significant difference is in the value of the pressure component of the propeller thrust, due to the difference of the flow field behind the thruster. Because of the different advance speed, the pressure on the propeller pressure side cannot increase as much at  $\beta = 10^\circ$  as in the other case. The ratio of viscosity and pressure components of the propeller torque are quite similar, with about 17 % viscous fraction at  $\beta = 10^\circ$  and 11 % at  $\beta = -10^\circ$ . Still, it is possible that the different propeller surface roughness between measurements and simulations may produce different flow and separation conditions in the critical beta range, which may increase the torque demand of the propeller, thus reducing the resulting thrust. Even after proper surface treatment (grinding, painting), the FFF 3D printed propeller blades will not be as smooth as the geometry used in the CFD simulations, as investigated in [36]. Further measurements should be taken to investigate this in more depth. The deformation of the propeller blades does not have a significant effect on the results, as demonstrated in [35].



**Fig. 9** Comparison of absolute pressure distribution on the suction side (a, b) and the pressure side (c, d) of the propeller.

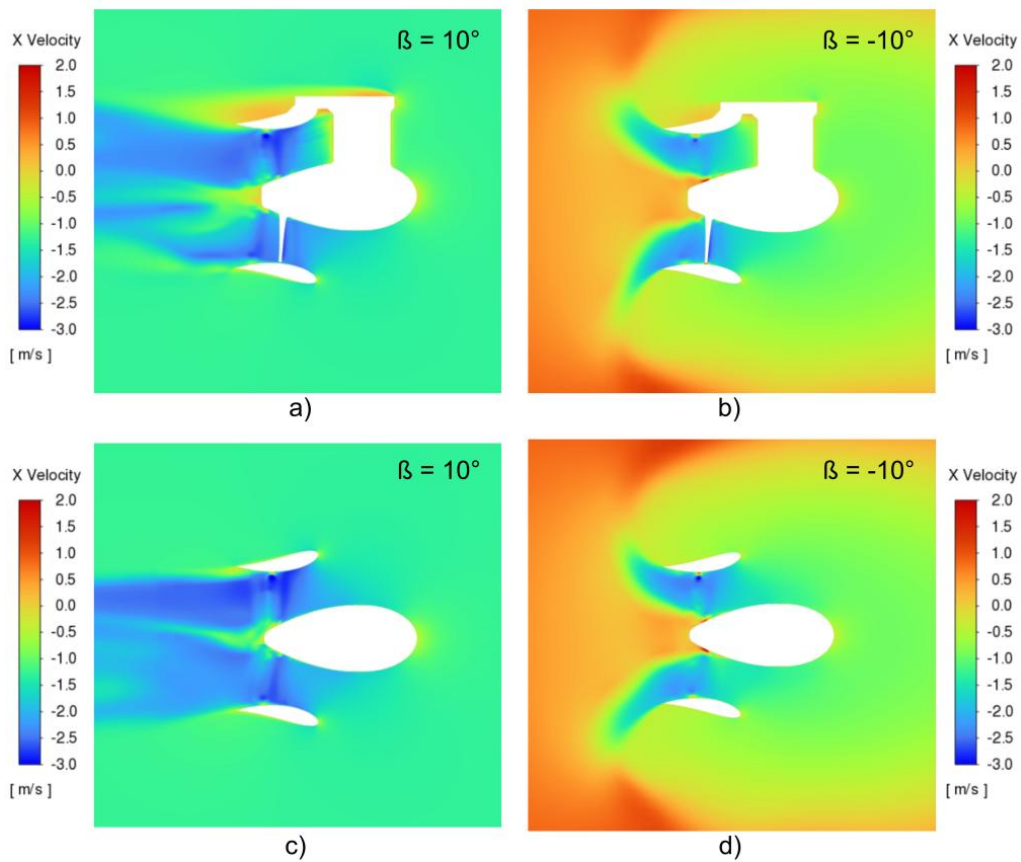


**Fig. 10** Comparison of axial velocity distribution in XZ plane (a, b) and XY plane (c, d).

It should be emphasized that the MRF method is mainly used for steady-state flow studies, which is not the case in the critical beta ranges. The use of the SM method could further improve the accuracy of the results in the critical conditions, but, as the results in the usual ranges  $\beta = [0^\circ, 20^\circ]$  and  $[180^\circ, 200^\circ]$  are already satisfactory accurate, and as the relatively low computation time is more important for the purposes of this paper, the results with MRF method is used for now. For more accurate simulations of the critical  $\beta$  ranges, the use of SM or overset methods with correspondingly small time-step is recommended and will be considered in future studies.

The results of the dynamic CFD simulations also show the largest deviation in the  $\beta = [-20^\circ, 0^\circ]$  and  $[160^\circ, 180^\circ]$  operating conditions, which can be up to 40 % in extreme cases. Of course, by reducing the variation of the input parameters for a given time, the accuracy could be increased, but this would increase the time required for the calculations excessively. Despite the less accurate results, it is very important to emphasise that by applying dynamic simulations, much more information can be obtained about the thruster hydrodynamic characteristics over the full  $\beta$  range. This is illustrated in Figure 11 where the results are plotted over the full  $\beta$  range. It is also important to highlight that, due to the dead zone of the electric motor and the fact that the maximum speed of the designed USV does not reach 3 m/s even in extreme cases, hardly any operating point is established in the range of  $\beta = [-150^\circ, -50^\circ]$  and  $[50^\circ, 150^\circ]$  under normal operation. Since the same motor and ESC were used in the experiments, it was not possible to perform measurements in this  $\beta$  range due to the ESC limitations mentioned in section 3.1.

The  $\beta = -90^\circ$  and  $90^\circ$  points are important operating points for  $n = 0$  rpm, which will be considered in the simulations, since these points represent the resistance of the thruster. As it was not possible to measure the propeller shaft torque directly, the deviations of the  $C_Q$  torque coefficient are only informative and further measurements would be needed for a more accurate validation. In summary, the dynamic CFD simulations show that for appropriate input parameters, when the sign of the advance speed and the propeller rotational speed are the same, the results are almost identical to those obtained with fixed input CFD simulations. In the range of  $\beta = [-20^\circ, 0^\circ]$  and  $[160^\circ, 180^\circ]$  the results are not accurate enough, for higher accuracy the input parameters must be changed more slowly, or the SM or overset method should be used with a smaller time-step. For a fast but reasonably accurate modelling, which provides data over the whole  $\beta$  range, a hybrid method will be used during development of the digital twin, where static measurement points in the critical  $\beta$  range are added to the dynamic simulation results.

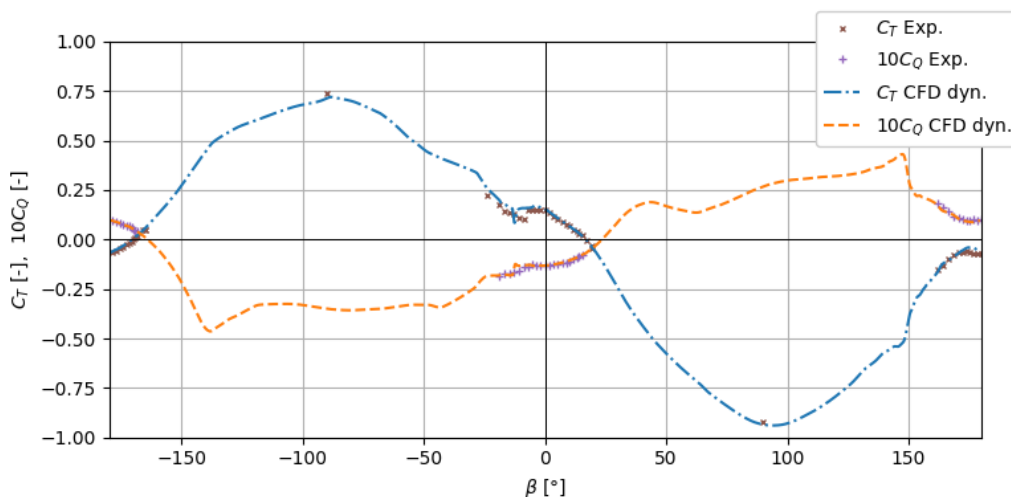


Fig. 11 Dynamic CFD results:  $C_T$  and  $C_Q$  in full  $\beta$  range

## 6. Digital twin of the thruster

In the future, the digital twin of the thruster will have two basic functions that will determine its structural design. Its primary purpose will be to enable the modelling of any USV, both dynamically and energetically, by integrating it into the open-source Gazebo simulation software. Thanks to the realistic manoeuvre

simulations, the control system and operation of USVs will be tested and developed in a safe environment before production. The efficiency of different control strategies and the energy consumption of the operational tasks will be tested. Another function could be if the digital twin of the thruster is used for diagnostics and troubleshooting. In this case the digital twin runs on the on-board computer of the USV and continuously compares the values measured by the sensors with the calculated values. By comparing the digital twin output data and the actual measured values (e.g. throttle, speed, current, etc.), the system performance can be checked, and in case of deviation, the fault can be indicated or even an intervention can be done (e.g. stop the thrusters). A deviation can be caused by e.g. seaweed, underwater vegetation, ropes, damaged propeller, or motor overheating, ESC failure, etc. Focusing on these tasks, the schematic of the digital twin presented in this work is shown in Figure 12. For ease of system integration, the inputs are directly the PWM [ $\mu\text{s}$ ] signal of the controller and the water velocity (advance speed:  $u_a$  [m/s]) at the propeller. The output can be thrust, speed and current, depending on the application. The first step in the execution of the digital twin is to calculate the operating point for the torque balance of the motor and propeller. This is computed by the *root\_scalar* function of the python SciPy module [37]. In the two torque equations (5) and arranged (3), only the rotational speed is variable, the parameters PWM and  $u_a$  are constant for each root finding. Knowing the resulting rotational speed, the total thrust is first calculated (arranged (4)). Then, the current draw is calculated based on the required torque, which is provided by the model generated from the underwater motor brake measurements (6). The ESC and PMSM model and the hydrodynamic model of the thruster are presented in the following sections.

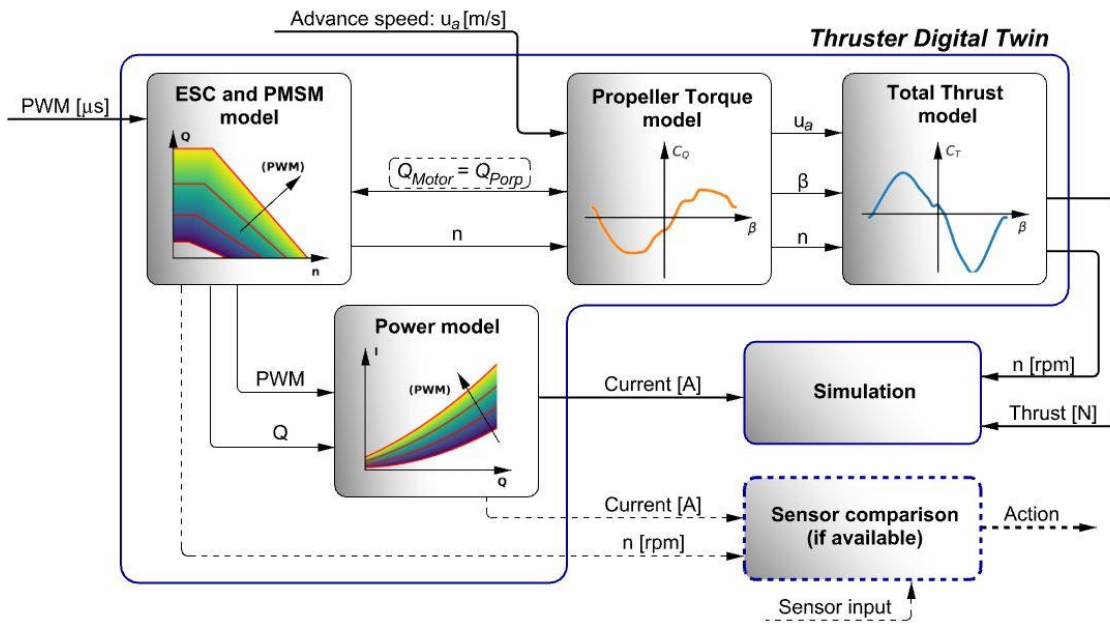


Fig. 12 Thruster digital twin system structure

### 6.1 ESC and PMSM model

The purpose of this subsystem is to determine the torque of the motor from the PWM control signal and the rotational speed resulting from the motor-propeller interaction. The current draw of the motor is calculated from the determined torque and the control PWM signal. Both relationships have been modelled using two-dimensional polynomial regression, with equations (5) and (6).

$$Q(n, PWM) = m_0 + m_1 \cdot n + m_2 \cdot PWM + m_3 \cdot n \cdot PWM + m_4 \cdot PWM^2 \quad (5)$$

$$I(Q, PWM) = a_0 + a_1 \cdot Q + a_2 \cdot PWM + a_3 \cdot Q \cdot PWM + a_4 \cdot Q^2 + a_5 \cdot PWM^2 \quad (6)$$

The dead zone and saturation of the motor rpm are handled by the program code using multi-layer comparisons. The final model is shown in Figure 13, where the motor torque is plotted as a function of rotational speed and PWM signal width. The energy consumption model is shown in Figure 14, where the

current draw is plotted as a function of torque and PWM signal width. It is worth highlighting that these models are only true if a 12 V power source is used (e.g. 3S LiPo battery). The parameters of the equations describing the models are given in Table 3.

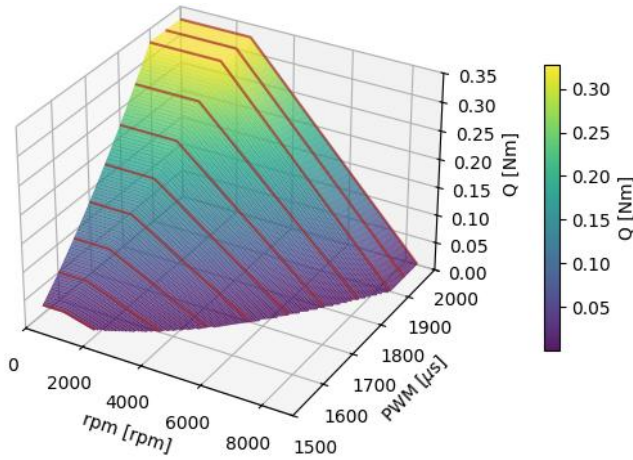


Fig. 13 Torque model of ESC and PMSM

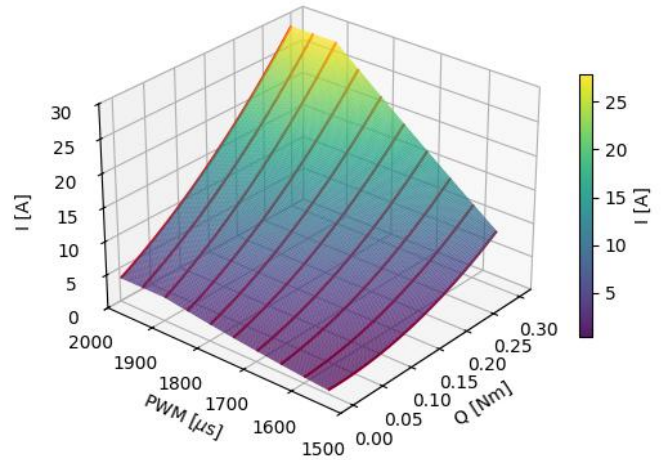


Fig. 14 Current model of ESC and PMSM

Table 3 ESC and PMSM model parameters

$m_0$	1.701	$a_0$	8.398
$m_1$	0.0001694	$a_1$	-249
$m_2$	-0.002991	$a_2$	-0.01617
$m_3$	-1.102e-07	$a_3$	103.6
$m_4$	1.232e-06	$a_4$	0.1577
		$a_5$	7.127e-06

## 6.2 Propeller model

The hydrodynamic model of the thruster was created by Fourier regression and interpolation of the validated CFD data. To ensure accuracy, the fixed input CFD results were used in the critical ranges  $\beta = [-20^\circ, 0^\circ]$  and  $[160^\circ, 180^\circ]$ , while dynamic CFD results were used otherwise. To perform high quality regression, it was necessary to use a Fourier series with at least 20 terms, which may require too much computation on computers with limited processing power. In these cases, much faster computation is possible by using interpolation on suitably filtered data (e.g. python Scipy PchipInterpolator [37]). A comparison of the two methods is shown in Figure 15. In python environment the time required for a given number of calculations using interpolation (with 200 data points) is 40 % less than using a 20 term Fourier series. Note that interpolation requires more memory to store the data, which is in the example below 600 floating-point (32 bit) numbers.

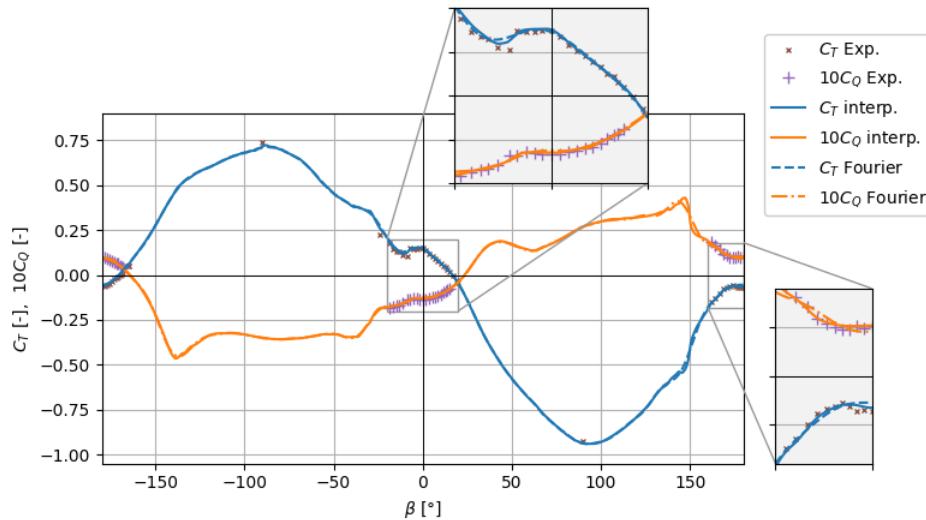


Fig. 15 Hydrodynamic model of the thruster

### 6.3 Operation and validation of the digital twin

When the created digital twin is used, the control PWM signal between 1000 and 2000  $\mu\text{s}$  is always required as input. The other required (but not necessarily essential) input is the water velocity arriving to the thruster in the direction of the propeller shaft. When using Gazebo simulation environment, this is typically equal to the longitudinal velocity of the vessel relative to water. For on-board observer configurations, an ultrasonic or mechanical water velocity sensor may be required, especially if the thruster is operating on rivers or in strong currents. For such applications, the resulting propeller rotational speed and current consumption are the most important outputs, because these values can be compared with sensor data. For manoeuvring simulations, the most important output of the digital twin is the thrust and the energy consumption. This allows a wide range of USV functionalities to be tested in a safe environment at low cost. The results of the variable input towing tank measurements were used to validate the developed digital twin and the ESC, motor, propeller interaction. The results of the measurements are shown in Figure 16, where the resulting propeller rotational speed is plotted as a function of advance speed and control PWM signal (blue thick lines). The rotational speed calculated with the digital twin, represented by the colormap surface with red grid lines, are also plotted in this figure.

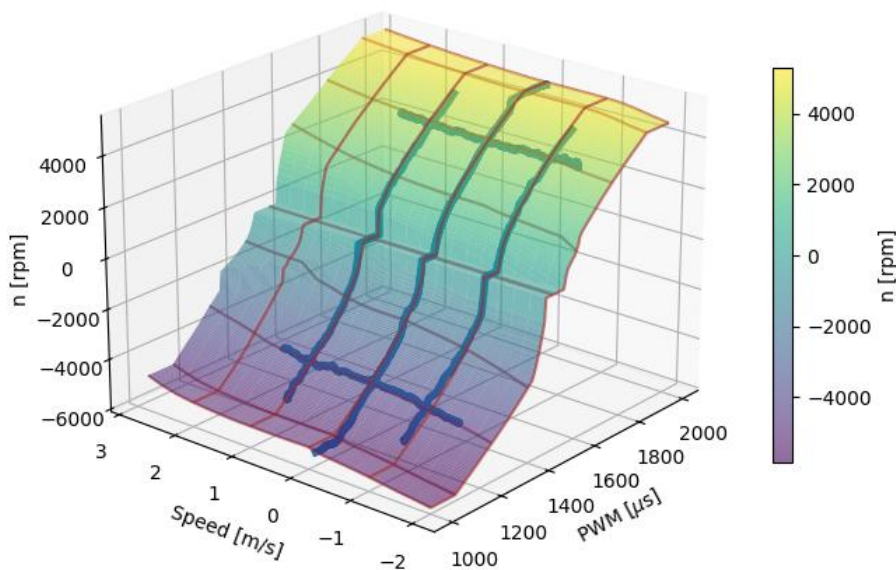


Fig. 16 Validation of the thruster digital twin

The absolute relative rpm error compared to the experimental data is 2.4 % in average outside the motor dead zone (rpm = 0). The larger error peaks typically occur in the large throttle zones, when PWM < 1200  $\mu$ s or PWM > 1300 $\mu$ s, when the maximum relative error does not exceed 18.1 % or 7.8 % respectively. The reason for this can depend on several factors, including different propeller surface quality, inaccuracies in CFD simulations and underwater motor bench tests, and simplifications introduced during the modelling process. It should be noted that the model does not consider that in the motor dead zone (0 % throttle around 1500  $\mu$ s) the propeller can spin up at high (absolute) advance speeds. Overall, it can be stated that the accuracy of the created digital twin is suitable for the objectives set in this study.

## 7. Conclusions

The created thruster digital twin is primarily intended to support the development of USVs for inland waterway and coastal environments. In practice, it is often not feasible or risky to test and perform control tuning of a USV equipped with expensive instruments and sensors. Thus, realistic simulations are becoming more and more important, especially in hazardous operating conditions e.g. flooding river, catastrophe, bad weather conditions, heavy traffic, etc. To allow the modelling presented in this paper to be easily performed on other geometries of thrusters, the results of CFD studies have been used for the hydrodynamic model. Towing tank experiments for the validation of CFD results are presented. Slowly varying input dynamic CFD simulations have shown that in the case where the sign of propeller rotational speed and advance speed are the same, the results are as accurate as if the simulations were performed at discrete input points. In the range  $\beta = [-20^\circ, 0^\circ]$  and  $[160^\circ, 180^\circ]$ , more time and more computational power is needed to stabilize the flow and converge the simulations. Different modelling method of propeller rotation is also suggested in these critical operating conditions using for example SM or overset methods. To achieve a faster but still reasonably accurate modelling, a hybrid method was used where static input measurement results are added to the dynamic simulation results in the critical  $\beta$  range. To accurately model the ESC, motor, propeller interaction, underwater brake tests of the thruster were performed. The input of the final digital twin is the PWM signal from the USV control computer and the water velocity at the propeller. Output is the resulting propeller rotational speed, thrust and current drawn by the ESC. The operation of the system was validated by towing tank tests, which showed that the accuracy of the digital twin meets the objectives. In summary, the created thruster digital twin is based on the results of CFD simulations validated by towing tank experiments and can be used for realistic and safe simulations of USVs or can be run on an on-board computer for diagnostic and prediction tasks. Future research goals include the investigation of digital positioning of under-actuated differential steering USVs, in strong current river environment, towing water quality sensors, pumps, sediment collector equipment or underwater cameras at different depths.

## REFERENCES

- [1] Lewicka, O., Specht, M., Stateczny, A., Specht, C., Dardanelli, G., Brčić, D., et al., 2022. Integration Data Model of the Bathymetric Monitoring System for Shallow Waterbodies Using UAV and USV Platforms. *Remote Sensing*, 14, 4075. <https://doi.org/10.3390/rs14164075>
- [2] Specht, C., Świtalski, E., Specht, M., 2017. Application of an Autonomous/Unmanned Survey Vessel (ASV/USV) in Bathymetric Measurements. *Polish Maritime Research*, 24, 36–44. <https://doi.org/10.1515/pomr-2017-0088>
- [3] Wajs, J., Kasza, D., 2021. Development of low-cost Unmanned Surface Vehicle system for bathymetric measurements. *IOP Conference Series: Earth and Environmental Science*, 684, 012033. <https://doi.org/10.1088/1755-1315/684/1/012033>
- [4] Sanjou, M., Shigeta, A., Kato, K., Aizawa, W., 2021. Portable unmanned surface vehicle that automatically measures flow velocity and direction in rivers. *Flow Measurement and Instrumentation*, 80, 101964. <https://doi.org/10.1016/j.flowmeasinst.2021.101964>
- [5] Brown, J., Tuggle, C., MacMahan, J., Reniers, A., 2011. The use of autonomous vehicles for spatially measuring mean velocity profiles in rivers and estuaries. *Intelligent Service Robotics*, 4, 233–244. <https://doi.org/10.1007/s11370-011-0095-6>
- [6] Katsouras, G., Dimitriou, E., Karavoltos, S., Samios, S., Sakellari, A., Mentzafou, A., et al., 2024. Use of Unmanned Surface Vehicles (USVs) in Water Chemistry Studies. *Sensors*, 24, 2809. <https://doi.org/10.3390/s24092809>
- [7] Jo, W., Hoashi, Y., Aguilar, L., Postigo, M., Garcia-Bravo, J., Min, B.-C., 2019. A Low-cost and Small USV Platform for Water Quality Monitoring. *HardwareX*, 6, e00076. <https://doi.org/10.1016/j.ohx.2019.e00076>

- [8] K, M., Adi N, S., Prayogo, N., Budiyo, A., 2009. Design and testing of underwater thruster for SHRIMP ROV-ITB. *Indian Journal of Marine Sciences*, 38, 338-345.
- [9] Raber, G.T., Schill, S.R., 2019. Reef Rover: A Low-Cost Small Autonomous Unmanned Surface Vehicle (USV) for Mapping and Monitoring Coral Reefs. *Drones*, 3, 38. <https://doi.org/10.3390/drones3020038>
- [10] Yang, L., Xiang, X., Kong, D., Yang, S., 2024. Small Modular AUV Based on 3D Printing Technology: Design, Implementation and Experimental Validation. *Brodogradnja*, 75 (1), 75104. <https://doi.org/10.21278/brod75104>
- [11] Ljulj, A., Slapničar, V., Brigić, J., 2022. Unmanned surface vehicle – Tritor. *Brodogradnja*, 73, 135–150. <https://doi.org/10.21278/brod73308>
- [12] Stanway, M.J., Stefanov-Wagner, T., 2006. Small-diameter ducted contrarotating propulsors for marine robots, in: *OCEANS 2006*, Boston, Massachusetts, United States. <https://doi.org/10.1109/OCEANS.2006.307030>
- [13] Su, S., Miao, Z., Zhao, Y., Song, N., 2024. Digitally twin driven ship cooling pump fault monitoring system and application case. *Brodogradnja*, 75(4), 75403. <https://doi.org/10.21278/brod75403>
- [14] Tanakitkorn, K., Phoemsapthawee, S., 2022. Impacts of thruster configurations on the task performance of an unmanned surface vehicle. *Ocean Engineering*, 256, 111465. <https://doi.org/10.1016/j.oceaneng.2022.111465>
- [15] Li, C., Jiang, J., Duan, F., Liu, W., Wang, X., Bu, L., Sun, Z., et al., 2019. Modeling and Experimental Testing of an Unmanned Surface Vehicle with Rudderless Double Thrusters. *Sensors*, 19, 2051. <https://doi.org/10.3390/s19092051>
- [16] Mikulec, M., Piehl, H., 2025. Development of a modified body force method for modelling azimuth thrusters in CFD-based manoeuvring simulations. *Ocean Engineering*, 319, 120171. <https://doi.org/10.1016/j.oceaneng.2024.120171>
- [17] Chen, W., Ma, J., Hu, J., Zhang, L., 2023. Numerical Simulation of Hydrodynamic Performance of Podded Propulsion under Maneuvering Condition. *Journal of Marine Science and Engineering*, 11, 874. <https://doi.org/10.3390/jmse11040874>
- [18] Bhattacharyya, A., Krasilnikov, V., Steen, S., 2016. Scale effects on open water characteristics of a controllable pitch propeller working within different duct designs. *Ocean Engineering*, 112, 226–242. <https://doi.org/10.1016/j.oceaneng.2015.12.024>
- [19] Liu, B., Vanierschot, M., Buysschaert, F., 2023. Optimization design of the duct of a rim-driven thruster using the adjoint approach. *Ocean Engineering*, 278, 114293. <https://doi.org/10.1016/j.oceaneng.2023.114293>
- [20] Liu, B., Ouyang, W., Yan, X., Vanierschot, M., 2024. Numerical Investigation of Hydrodynamic Characteristics of a Rim-Driven Thruster Coupled with an Underwater Vehicle. *Journal of Marine Science and Engineering*, 12, 1838. <https://doi.org/10.3390/jmse12101838>
- [21] Song, B., Wang, Y., Tian, W., 2015. Open water performance comparison between hub-type and hubless rim driven thrusters based on CFD method. *Ocean Engineering*, 103, 55–63. <https://doi.org/10.1016/j.oceaneng.2015.04.074>
- [22] Touzout, W., Benmoussa, Y., Benazzouz, D., Moreac, E., Diguët, J.-P., 2021. Unmanned surface vehicle energy consumption modelling under various realistic disturbances integrated into simulation environment. *Ocean Engineering*, 222, 108560. <https://doi.org/10.1016/j.oceaneng.2020.108560>
- [23] Liu, J., Yue, Q., Wu, S., Yue, X., 2024. Hydrodynamic shape optimization of an autonomous and remotely-operated vehicle via a multi-surrogate model. *Brodogradnja*, 75(3), 75301. <https://doi.org/10.21278/brod75301>
- [24] Wang, Z., Wei, Z., Yu, C., Cao, J., Yao, B., Lian, L., 2023. Dynamic modeling and optimal control of a positive buoyancy diving autonomous vehicle. *Brodogradnja*, 74(4), 19-40. <https://doi.org/10.21278/brod74102>
- [25] Cosgun, T., Esenkalan, M., Kinaci, O.K., 2024. Four-quadrant propeller hydrodynamic performance mapping for improving ship motion predictions. *Brodogradnja*, 75(3), 75306. <https://doi.org/10.21278/brod75306>
- [26] Pivano, L., Smogeli, O., Johansen, T., Fossen, T., 2007. Experimental Validation of a Marine Propeller Thrust Estimation Scheme. *Modeling, Identification and Control*, 28. <https://doi.org/10.4173/mic.2007.4.2>
- [27] Duecker, D.A., Bauschmann, N., Hansen, T., Kreuzer, E., Seifried, R., 2020. HippoCampusX – A Hydrobatic Open-source Micro AUV for Confined Environments, in: *2020 IEEE/OES Autonomous Underwater Vehicles Symposium (AUV)*, St. Johns, Newfoundland and Labrador, Canada. <https://doi.org/10.1109/AUV50043.2020.9267949>
- [28] Hoffer, A.E., Petrov, I., Pyrhönen, J.J., Tapia, J.A., 2021. Stainless-Core Submersible Permanent Magnet Synchronous Machine. *IEEE Access*, 9, 28089–28100. <https://doi.org/10.1109/ACCESS.2021.3058593>
- [29] Kiss-Nagy, K., Simongáti, G., Hargitai, C.L., 2024. Simulation of inland passenger vessel mooring maneuvers to improve safety and efficiency of inland navigation. *XIV International Conference on Transport Sciences: Navigating the way of the future*, Győr, Hungary, pp. 122-134.
- [30] Paravisi, M., H. Santos, D., Jorge, V., Heck, G., Gonçalves, L.M., Amory, A., 2019. Unmanned Surface Vehicle Simulator with Realistic Environmental Disturbances. *Sensors*, 19, 1068. <https://doi.org/10.3390/s19051068>
- [31] Bingham, B., Agüero, C., McCarrin, M., Klamo, J., Malia, J., Allen, K., et al., 2019. Toward Maritime Robotic Simulation in Gazebo. *OCEANS 2019 MTS/IEEE SEATTLE*. Seattle, Washington, United States. <https://doi.org/10.23919/OCEANS40490.2019.8962724>

- [32] Keat, C.C., Arshad, M.R., Din, S., 2022. Navigation and control design for catamaran autonomous surface vessel in Gazebo environment, *Journal of Engineering Science and Technology*, 17, 4335-4354.
- [33] Vicent, X., Dhanak, M.R., 2024. Performance and Comparison of PID-Based Techniques for USV Navigation. *OCEANS 2024 - Halifax*. Presented at the *OCEANS 2024*, Halifax, Canada. <https://doi.org/10.1109/OCEANS55160.2024.10754061>
- [34] Xiao, G., Zheng, G., Tong, C., Hong, X., 2023. A Virtual System and Method for Autonomous Navigation Performance Testing of Unmanned Surface Vehicles. *Journal of Marine Science and Engineering*, 11, 2058. <https://doi.org/10.3390/jmse11112058>
- [35] Kiss-Nagy, K., Simongáti, Gy., Ficzere, P., 2024. Investigation of 3D Printed Underwater Thruster Propellers Using CFD and Structural Simulations. *Periodica Polytechnica Mechanical Engineering*, 68, 70–77. <https://doi.org/10.3311/PPme.23795>
- [36] Kónya, G., 2024. Investigating the Impact of Productivity on Surface Roughness and Dimensional Accuracy in FDM 3D Printing. *Periodica Polytechnica Transportation Engineering*, 52, 128–133. <https://doi.org/10.3311/PPtr.22952>
- [37] Virtanen, P., Gommers, R., Oliphant, T.E., Haberland, M., Reddy, T., Cournapeau, D., et al., 2020. SciPy 1.0: fundamental algorithms for scientific computing in Python. *Nature Methods*, 17, 261–272. <https://doi.org/10.1038/s41592-019-0686-2>